Int J Mech Mater Des (2016) 12:353–373
DOI 10.1007/s10999-015-9311-4

Optimization of operating conditions for a double-row tapered roller bearing

Ruben Lostado · Ruben Escribano García · Roberto Fernandez Martinez

Received: 23 February 2015 / Accepted: 19 May 2015 / Published online: 29 May 2015

Abstract This paper proposes a methodology that combines the Finite Element Method and multiple response surface optimization to search for the optimal operating conditions of a double-row Tapered Roller Bearing (TRB) that has a Preload (P), radial load (F_r), axial load (F_a) and torque (T). Initially, FE models based on a double-row TRB are built and validated in the basis of experimental data and theoretical models. Three of the most important parameters used in the design of TRB were obtained from a simulation of the FE models with a combination of several operating conditions that were previously selected in accordance with a design of experiments. The design parameters are: contact stress radio for both rows of rollers (S_1 and S_2), maximum deformation of the outer raceway (α_{max}), and the difference between the gaps of the inner raceways ($\Delta\delta$) or misalignment. Based on the results of the FE simulations, quadratic regressions models are generated that use the response surface method to predict the design parameters when new operating condition are applied. Then, a multi-response optimization study based on these models and using desirability functions is conducted. It is concluded that the accuracy of the results demonstrates that this methodology may be used to search for the optimal operating condition in a double-row TRB.

Keywords Double row tapered roller bearing · Finite element method · Design of experiments · Multiple response surface optimization

List of symbols

l_t	Rollers' effective length (mm)
d_m	Mean diameter of tapered roller (mm)
D_{max}	Diameter of tapered roller at large end (mm)
D_{min}	Diameter of tapered roller at small end (mm)
D_m	Bearing pitch diameter (mm)
D_i	Bore diameter (mm)
D_o	Outer diameter (mm)
L	Longitude of the bearing (mm)
Z	Number of rollers
b_o	Semi minor axis of the projected contact ellipse (mm)
K_n	Load deflection factor
σ	Contact normal stress (MPa)
α	Contact angle (°)
α_i	Inner raceway-roller contact angle (°)
α_o	Free contact angle (°)

R. Lostado (✉)
Mechanical Engineering Department, University of La Rioja, Logroño, Spain
e-mail: ruben.lostado@unirioja.es

R. Escribano García
Built Environment and Engineering, Leeds Beckett University, Leeds, UK
e-mail: ruben.escribanogarcia@gmail.com

R. Fernandez Martinez
Electrical Engineering Department, University of Basque Country UPV-EHU, Bilbao, Spain
e-mail: roberto.fernandezm@ehu.es

α_R	Tapered roller included angle (°)
$\sum \rho_o$	Curvature sum (mm^{-1})
MAPE	Mean Absolute Percentage Error
RMSE	Root Mean Square Error

1 Introduction

This paper attempts to demonstrate how the combination of the Finite Element Method (FEM) and the Multiple Response Surface (MRS) optimization can be used to obtain the optimal operating conditions in the design phase of a double-row TRB. TRBs are mechanical devices that are used in many industrial applications. Basically, the TRB is formed by a pair of inner raceways that are separated by a gap of constant distance (δ), an outer raceway, and a group of tapered rollers that are located between the inner and outer raceways. This type of mechanical device is designed to support preload (P), axial (F_a), radial (F_r) and torque (T) loads (operating conditions) that are applied under both static and dynamic conditions. An incorrect combination of these operating conditions can result in high contact stresses (even higher than 1000 MPa) on the TRB rolling elements. This can cause significant local deformations (α_{max}) and defects, such as pitting and fatigue spalling (Harris and Kotzalas 2006). In addition, if the operating conditions that are applied to the TRB differ from the values that the manufacturer provided, the distribution of contact stresses on the outer raceway in some areas of contact can become nil, cause the rollers to detach from the outer raceways (Nagatomo et al. 2012). Also, a torque that greatly exceeds that recommended by the manufacturer, combined with a reduced preload, may cause the rotation of one of the raceways and a variation of δ that causes the TRB works with difficulty. In this sense, the design, optimization and determination of optimum operating conditions of TRB are mainly based on parameters such as contact stresses, local deformation in the raceways, misalignments and distribution of forces on the rolling elements (Harris and Kotzalas 2006). These parameters are generally studied individually in the design phase of the bearings. However, this form of study has the disadvantage of not obtaining a complete and realistic design of the mechanical device. The novel aspect of this work is that the combination of FEM and the Multiple Response Surface (MRS) optimization could be used to obtain the optimal operating conditions in the design phase of a double-row TRB, while considering at the same time three of the most important design parameters:

- The contact stress radio that is calculated using the maximum contact normal stress [obtained in the top side of the outer raceway (S_{top})] and the minimum contact normal stress [obtained in the bottom side of the outer raceway (S_{bottom})].
- The difference between the gaps obtained in the top and bottom sides of the inner raceways (δ_{top} and δ_{bottom}) or misalignment.
- The local deformation of the contact surface of the outer raceway (α_{max}).

The optimal operating conditions in a double-row TRB can be achieved by adjusting the values of P, F_a, F_r and T loads when: (1) do not exceed a fixed threshold of contact stress radio for both rows of rollers, (2) that the difference between the gaps or misalignment should be as reduced as much as possible, and (3) that the local deformation on the contact surface of the outer raceway (α_{max}) not exceed the maximum elastic deformation value. Due to the complexity of finding the optimal operating condition of double-row TRB when three of the most important parameters used in the design phase of TRB are fulfilled simultaneously, 3D FE models, including the P, F_a, F_r and T loads, are developed. The results obtained from these FE models are used (1) to generate quadratic regression models, (2) to predict new operating conditions covering the entire space of possibilities, and (3) to obtain the optimal operating condition of a double-row TRB using MRS with desirability functions.

1.1 Use of the FEM for modeling and optimizing bearings

The FEM is commonly used to design and optimize mechanical devices since it reduces the number of physical prototypes and experiments needed during the design phase (Shigley et al. 2004). In this way, FEM has been applied by many researchers to design bearings. The object of its application is to reduce the produce's cost by experimental tests once the prototypes have been manufactured.

The FEM, combined with experimental data, has been used to identify and characterize the static and dynamic properties of the bearings. In this sense, Arora et al. (2010) and Arora et al. (2011) used a combination of FEM and experimental data to find the structural characteristics of radial Air-foil bearings and axial Air-foil bearings respectively. The proposed method uses the natural frequencies and modal shapes of the complete bearing to identify structural characteristics of the mechanical device. Also, FEM has been used to obtain the bearing stiffness of a wide range of bearing types and parameters (Guo and Parker 2012). This proposed method was validated by experiments in the literature and is compared to analytical models. Despite the obvious advantages of using the FEM, there are some disadvantages when this method is applied to design mechanical components, such as convergence problems, due to the adjustment of the mesh size, especially if the FE model includes mechanical contacts. It is well known that if the contact surface between the bodies is limited and the mesh size is large, the number of nodes in that contact surface will be reduced and the calculation of contact stresses will not be accurate (Zhang et al. 2003; Demirhan and Kanber 2008). Thus, it is concluded that the FEM is not an appropriate method to use in design and optimization processes if a considerable number of FE simulations are required and the FE models includes nonlinearities. One strategy to reduce the number of simulations required for modeling and optimizing the FE models is to build regression models, such as those based on soft computing techniques and Response Surface Methodology (RSM), that learn from the most characteristic samples obtained from FEM simulations and to use their outputs as a substitute of new FE simulations. RSM is a group of mathematical techniques that utilize a low-degree polynomial function to model the relationships between the independent variables (input variables) and one or more response variables (output variables). Sometimes, these polynomial functions do not provide good results in complex problems that have many nonlinearities and a high number of inputs as the polynomials should be continuous functions. In contrast, soft computing techniques is the set of techniques that are used to explore databases automatically or semi-automatically in order to find patterns, trends or rules that explain the behavior of the data in a given context (Borgelt et al. 2013). Models based on soft computing techniques normally require a larger amount of data to obtain a good model than that required for RSM (Escribano et al. 2014; Lostado et al. 2014). Using soft computing techniques, Lostado et al. (2009) studied the contact pressure on a hub where it was mounted a double-row TRB. In this case, different types of regression techniques were used to predict the distribution of the contact pressures on the hub as function of a preload, a load and a friction coefficient. Applying these regression techniques usually requires a large number of data to generate models with an appropriate generalization capability.

1.2 Response surface method for modeling and optimizing problems

In many cases, the RSM is used to model experimental responses. However, it recently is being used in combination with other techniques (i.e., FEM) to optimize products and industrial processes. RSM is an approximate optimization method that looks at various controllable and independent variables (inputs) and their responses (outputs), in order to identify the combination of inputs that provide the best response [Eq. (1)] (Box and Wilson 1951).

$$Y = f(x_1, x_2, x_3, \ldots, x_k) \tag{1}$$

where Y is the response for the experiments and $(x_1, x_2, x_3, \ldots, x_k)$ are the vectors of input. To optimize the response Y, it is necessary to find an approximation functional relationship between the inputs and the response surface. A second-order polynomial is the functional relationship used by RSM [(Eq. (2)] in this kind of work.

$$Y = b_0 + \sum_{i=1}^{n} b_i \cdot X_i + \sum_{i=1}^{n} b_{ii} \cdot X_i^2 + \sum_{i=1}^{n-1} \sum_{j=i+1}^{n} b_{ij} \cdot X_i \cdot X_j + \varepsilon \tag{2}$$

where the first summation is the linear part, the second is the quadratic part, the third is the product of pairs of all inputs of the polynomial, and ε is the approximation error. The values of the coefficients b_0, b_i, b_{ii} and b_{ij} are calculated using regression analysis to determine the relationship between inputs and outputs. Also, the terms that are selected to form the equation are chosen

according to their levels of significance (Gelman 2005). One computes this level by using the analysis of variance (ANOVA) and selecting terms according to the p value obtained. When a problem has more than one output, as in this work, the optimization problem can be solved using MRS (Derringer and Suich 1980). In this sense, Harrington developed the desirability functions to obtain a compromise between the different outputs [Eqs. (3) and (4)], and the overall desirability, which is defined as the geometric mean of the desirability of each output [Eq. (5)] (Harrington 1965).

$$d_r^{max} = \begin{cases} 0 & \text{if } f_r(X) < A \\ \left(\dfrac{f_r(X) - A}{B - A}\right)^S & \text{if } A \le f_r(X) \le B \\ 1 & \text{if } f_r(X) > B \end{cases} \quad (3)$$

$$d_r^{min} = \begin{cases} 1 & \text{if } f_r(X) < A \\ \left(\dfrac{f_r(X) - A}{A - B}\right)^S & \text{if } A \le f_r(X) \le B \\ 0 & \text{if } f_r(X) > B \end{cases} \quad (4)$$

$$D = \left(\prod_{r=1}^{R} d_r\right)^{1/R} \quad (5)$$

In these equations, parameters A and B correspond to the limits of the inputs range, S is an exponent that determines how important it is to reach the target value, X corresponds to the input vector, and f_r is the polynomial function that is used to predict the response.

1.3 Combining FEM and MRS to optimize mechanical problems

For decades, many researchers have used the FEM as an alternative in attempting to reduce the costs during the design and optimization phases of mechanical problems. In this work, we show that FEM has a disadvantage of requiring a large amount of computational time when the studied problem has a nonlinear behavior. In contrast, RSM method tends to be immune to computational cost, as it provides a crude approximation for the same problem modeled with FEM (Marwala 2010). In this sense, the combination of RSM when the optimization involves several features and FEM has been used extensively to optimize industrial processes. Thus, for example, Bahloul et al. (2006) develops a 3D FE model for the prediction of the punch load and the stress distribution during the wiping-die bending process. In this work, the FE simulation is carried out through ABAQUS/Standard code, and the prediction of the punch load is performed using RSM to optimize the values of the main parameters involved in the bending process. Moreover, Zeng et al. (2009) combines RSM with FEM for optimizing the design of roll profiles for cold roll forming. In this case, the spring-back angle is considered to be an objective function and the edge membrane longitudinal strains is considered as constrain condition to ensure high forming accuracy with the minimum roll diameter of the forming process. Yanhui et al. (2010) improved the deformation homogeneity in aerospace forgings and Di Lorenzo et al. (2010) developed an optimization strategy for hydro-forming process design. In these research studies, a combination of FEM and RSM were used to model and optimize both processes. More recently, Azaouzi et al. (2012) studied an optimization approach to design a multi-step stamping tool while using a combination of RSM and FEM. Other authors also have used these methods to optimize the design of buildings. In this regard, del Coz Diaz et al. (2014) used RSM and FEM to develop predictive models to simulate and optimize the heat transfer process in buildings.

In the current paper, regression techniques using the results of FE analysis are applied to model S_1, S_2, $\Delta\delta$, and α_{max} when P, F_a, F_r and T are acting under static conditions on a double-row TRB. These models are based on polynomial regression techniques, and were built using RSM. Since TRB has more than one output to be optimized (S_1, S_2, $\Delta\delta$ and α_{max}), the optimization problem is solved by using MRS by means of desirability functions. Two criteria, Mean Absolute Percentage Error (MAPE) and Root Mean Square Error (RMSE), are used to determine the accuracy of the regression models and in the adjustment process of the FE models.

2 Modeling the double-row TRB using FEM

During the process, all FE models of the double-row TRB are considered to be symmetrical three-dimensional models to reduce the computational cost. The FE models proposed includes the outer raceway, the inner

raceways, the tapered rollers and the hub on which the TRB is mounted (Fig. 1a). The FE models are assembled from a combination of elements with 8 and 6 nodes formulated in linear shape functions. The coefficient of friction between the hub and the inner raceway is considered to be 0.2, whereas the coefficient between the rollers and the inner raceway and between the rollers and the outer raceway is considered to be 0.001 (Demirhan and Kanber 2008). Raceways and rollers are modeled using linear elastic and isotropic steel with a Young's modulus (E) equal to 208 GPa and a Poisson's ratio (ν) of 0.29. The hub is modeled on the basis of E = 200 GPa and ν = 0.29 (Demirhan and Kanber 2008). For all simulated FE models, the contact detection method used was the segment-to-segment method (MSC Marc User's Guide 2010). In contrast to the classical method of contact detection node-to-segment method, the segment-to-segment method is a consistent and stable method, and is able to easily pass the patch test (El-Abbasi and Bathe 2001). Also, the segment-to-segment method is able to reduce the error in calculating contact stresses with a mesh refinement (Meguid and Czekanski 2008; Zavarise and De Lorenzis 2009). The numerical technique used to solve the mechanical problem was the solver constraints technique. This technique does not require any special element to be placed at the points of contact, and the algorithm automatically detects nodes making contact and generates the appropriate constrains to ensure that no penetration occurs. Also, the friction model used in this case was the bilinear coulomb friction stick slip model. It was a quasi-static problem in which the movements between the different contact surfaces were practically negligible.

In this case, the FE models were adjusted and validated using radial loads F_r and preloads P well-known by this way: First, the mesh size in the contact area between the outer raceway and the tapered roller was adjusted comparing the normal contact stress obtained by the FE model and by a theoretical model based on the Hertz's theory. Then and once the mesh size was adjusted, the relative displacements between inner and outer raceway obtained by the FE model were compared to the results obtained in a test bench. These test results were used to ensure that the mesh size of the FE model and the coefficients of friction and elastic properties (E and ν), were perfectly defined. The following subsection shows the procedure to adjust and validate the FE models.

2.1 Adjustment of TRB based on the mesh size of raceways and rollers

One of the main difficulties in solving mechanical contact by the use of FEM is to obtain realistic contact stresses. It is well known that if the contact surface between the FE models is low and the mesh size is very

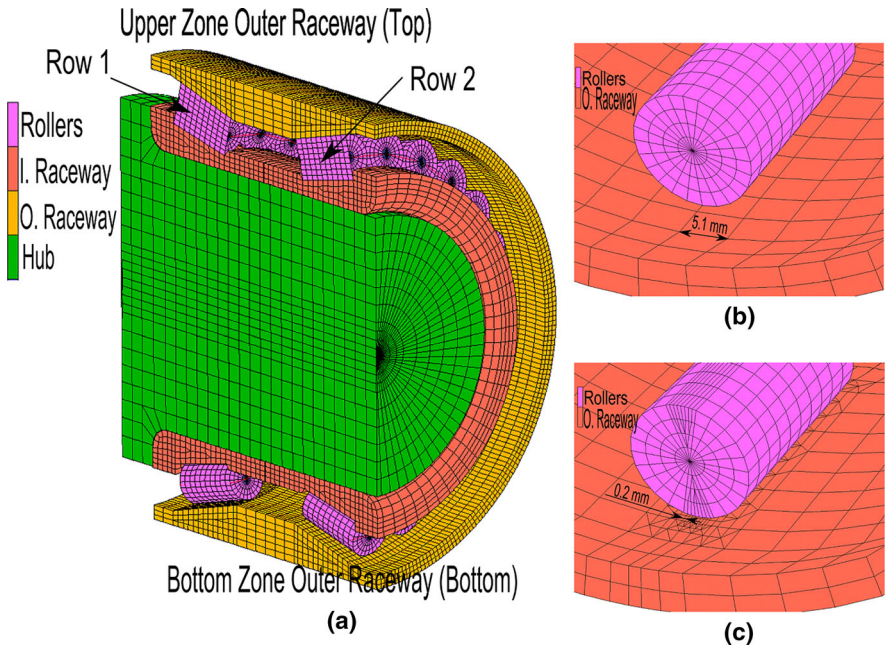

Fig. 1 FEM of the TRB: **a** Different component parts of the TRB, **b** Initial mesh of size 5.1 mm. **c** Final mesh of size 0.2 mm

large, the number of nodes in the contact surface is smaller and therefore the contact stresses obtained by this method does not are accurate (Feng and Prinja 2001). In this respect, researchers have studied how mesh size affects the contact stresses in the contact zone. For example, (Satyanarayana and Melkote 2004) studied the influence of the element size on the contact stress between ball bodies and flat surfaces. Similarly, Demirhan and Kanber (2008) developed two dimensional FE models based on cylindrical roller bearings and studied the influence of element size on the contact stress. The FE models are validated experimentally by two methods. One was by using theoretical models based on Lundberg's and Hertz's theory to calculate the contact stresses in the outer raceways (Lundberg and Sjövall 1958; Hertz 1896). The other method was by determining experimentally the relative displacement between the inner and outer raceways of the cylindrical roller bearings. The contact stresses obtained from the theoretical model based on Hertz's theories are calculated from the force applied to the cylindrical rollers, which is obtained after FE models are simulated. The convergence of the FE models based on the cylindrical roller bearings are achieved and considered to be valid when the results of the contact stresses and displacements obtained by the FE models proposed did not differ significantly from those results obtained, theoretically and experimentally respectively. In the current paper, and in a way that is similar to Demirhańs work, the mesh size of raceways and rollers were adjusted by comparing the contact stress obtained from the FE models and those obtained from the theoretical model based on Hertz's theories. Because the contact detection method that was proposed in this case for all FE models was the "segment to segment" method, it was possible to reduce the error in calculating the contact stresses with a mesh refinement (Zavarise and De Lorenzis 2009). In this case, FE models with localized fine mesh sizes in the contact area were created successively with increasingly smaller mesh size (mesh refinement) until the contact stresses on these FE models on the outer raceway did not differ significantly from the results obtained by theoretical models based on the Hertz's theory (Demirhan and Kanber 2008). This study concentrated on the contact zone (upper and bottom zones of the outer raceway) for both rows of rollers (Fig. 1b). The loads used for adjusting the mesh size of the FE model by comparison to theoretical models were P with 300, 400, 500, and 600 N and an F_r equal to 2000 N. The theoretical models, in which the FE models were compared, were based on the Hertz's theory for cylindrical bodies (Hertz 1896). Equation (6) shows how to calculate the contact normal stress σ on the outer raceway based on Hertz's theory (Fig. 2a).

$$\sigma = \frac{2 \cdot Q}{\pi \cdot l_t \cdot b_o} \tag{6}$$

In this equation, b_o is the width of the contact area, l_t is the rollers' effective length, and Q is the normal force on each tapered roller that is obtained directly from the FE model when the preload P (300, 400, 500, and 600 N) and F_r (2000 N) are simulated. Similarly, b_o is calculated by using Eqs. (9), (10) and (11), where $\sum \rho_o$ is the radii of curvature, D_m is the bearing pitch diameter, d_m is mean diameter of tapered roller, and α_o is the free contact angle.

$$b_o = 3.35 \cdot 10^{-3} \left(\frac{Q}{l_t \cdot \sum \rho_o} \right)^{1/2} \tag{7}$$

$$\sum \rho_o = \frac{1}{D_m} \left[\frac{2}{1 + \gamma_o} \right] \tag{8}$$

$$\gamma_o = \frac{D_m \cdot \cos \alpha_o}{d_m} \tag{9}$$

The particular geometrical dimensions of the studied TRB are: D_i (Bore diameter) = 78 mm, D_o (Outer diameter) = 130 mm, L (Longitude) = 90 mm, and Z (Number of rollers) = 25, α (Contact angle) = 14.07°, α_o (Free contact angle) = 15.7°, α_R (Tapered roller included angle) = 3.25°, α_i (Inner raceway-roller contact angle) = 12.45°, l_t (Rollers' effective length) = 20.9 mm, D_m (Mean diameter of tapered roller) = 11.925 mm, D_{max} (Diameter of tapered roller at large end) = 12.5 mm, D_{min} (Diameter of tapered roller at small end) = 11.35 mm, and d_m (Bearing pitch diameter) = 102.4 mm. Figure 2(b) shows the main geometrical dimensions of a double-row TRB (Harris and Kotzalas 2006).

Then, like the work performed by Illera et al. (2014) to set FE models in contact problems, the FE models based on the TRB are considered to be valid when the computational costs of each simulation are not excessive, and when:

$$\forall y_i \,/\, MAPE_{yi} < \varphi_{yi} \tag{10}$$

where y_i is the adjustment parameter and corresponds to the mesh size of the elements of the contact area.

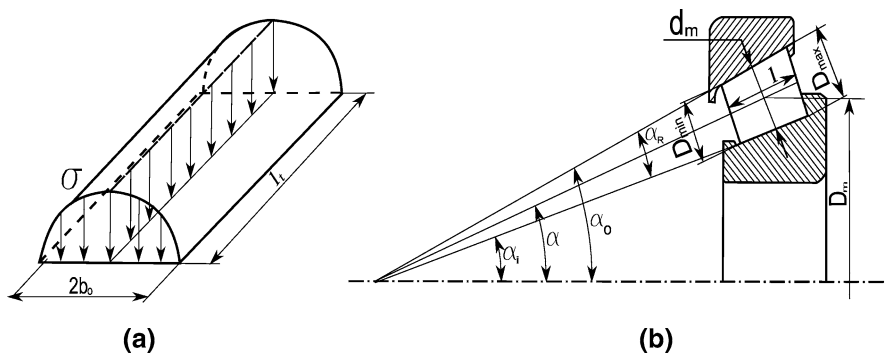

Fig. 2 **a** Theoretical distribution of contact stresses between the roller and the flat surface, **b** Main geometrical dimensions of a double-row TRB (Harris and Kotzalas 2006)

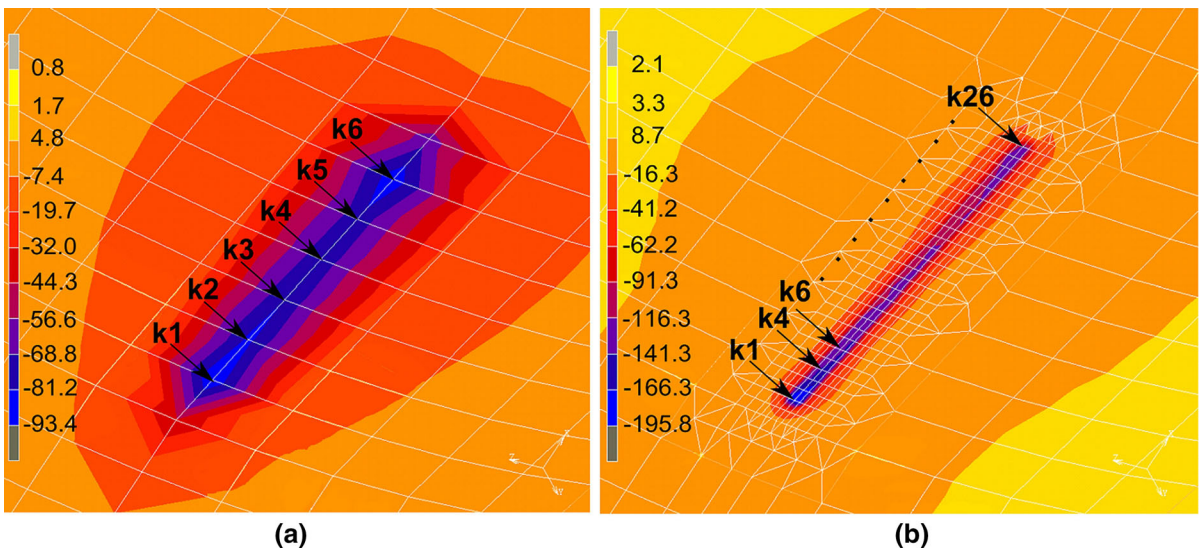

Fig. 3 Contact stresses on the *upper zone* of the outer raceway that correspond to the first row of rollers when the mesh size is: **a** 5.1 mm **b** 0.2 mm

Also, φ_{yi} is a previously established threshold and $MAPE_{yi}$ is the error that is defined as Eq. (11).

$$MAPE_{yi} = \frac{1}{m}\sum_{k=1}^{m}\left|\frac{Y_{yi\ FEM} - Y_{yi\ TH}}{Y_{yi\ TH}}\right| \tag{11}$$

where, $Y_{yi\ FEM}$ and $Y_{yi\ TH}$ are the contact stresses obtained from the FE model and the theoretical model, respectively, on the contact zone (upper and bottom zones of the outer raceway) of both rows of rollers and for each different combination of P and F_r. k is one of each result obtained for the nodes that belong to the localized contact zone and m is the total number of nodes considered at each mesh size. Figure 3 shows the contact stresses localized in the upper zone of the outer raceway when the mesh sizes are 5.1 and 0.2 mm. In this case, eight computers with Intel Xeon Processor, CPU 3.4 GHz (2 processors) and 10.00 GB (RAM), were used to simulate the FE models.

Table 1 shows the MAPE calculated with Eq. (11) to adjust the mesh of the FE models when P is 300, 400, 500, and 600 N; F_r is 2000 N; and the mesh sizes are 5.1, 1.0 and 0.2 mm. Table 1 shows the results obtained for the upper zone of the outer raceway in the first row of rollers. It also shows the average computational time to simulate each FE model with its corresponding mesh density.

In this study, the thresholds that are considered to be valid are $\varphi = 6\,\%$ for MAPE and 14,400 min (10 days) for maximum computational cost. According to Table 1, MAPE is lower than the threshold considered for all ($\varphi = 6\,\%$) P: 4.58, 4.68, 4.78, and 4.88 %). The average computational time is 11,952 min (8.3 days). Similarly, the MAPE was

Table 1 MAPE and computational cost of the FE models during the mesh density adjustment of the upper zone of the outer raceway that corresponds to the first row of rollers

Mesh size (mm)	MAPE (%)				Computational time (min)
	P = 300 N (%)	P = 400 N (%)	P = 500 N (%)	P = 600 N (%)	
5.1	53.6	53.37	52.86	52.34	6,912
1.0	22.34	22.56	22.64	22.68	8,496
0.2	4.58	4.68	4.78	4.88	11,952

calculated for the upper zone of the outer raceway that corresponds to the second row of rollers and for the bottom zone of the outer raceway to both rows of rollers and to each different combination of P and F_r when the mesh sizes were 5.1, 1.0 and 0.2 mm. For all these latter cases studied, when the mesh size was 0.2 mm, the computational time and the MAPE obtained were, respectively, <6 % and 14,400 min. In addition, all of the most important parameters used to determine the quality of the mesh were fulfilled strictly for all mesh sizes proposed and for all loads applied (Kelly et al. 1983). So, for example, the aspect ratio (defined as the ratio of the longest edge of an element to its shortest edge) never exceeded a value of 5:1 for any of the elements of the meshes studied. The Jacobian factor was always greater than 0.6 so that elements' zero volume did not exist, and the skew angles were less than 45° for all meshes and loads studied.

According to these criteria, the FE models selected had a mesh size equal to 0.2 mm in the contact zone (upper and bottom zones of the outer raceway) of both rows of rollers. Also, the coefficients of friction ($\mu = 0.2$ and $\mu = 0.001$) and elastic properties ($E_{Rollers} = 208$ GPa, $\nu_{Rollers} = 0.29$; $E_{Hub} = 200$ GPa and $\nu_{Hub} = 0.29$) proposed for the adjustment of TRB that were based on the mesh size of raceways and rollers were considered to be valid.

2.2 Adjustment of TRB based on relative displacements of the raceways

Once the mesh size, the coefficients of friction and the elastic properties where fixed and considered to be valid, the relative displacements between the inner and outer raceways that were obtained by the FE model were compared to the results obtained on the test bench. This study was conducted primarily to determine if the stiffness of the proposed FE models were very similar to that obtained experimentally for the TRB studied. The relative displacements between inner and outer raceway for each of the combinations of P and F_r were obtained experimentally from a test bench and also from the FE models based on the TRB proposed once the mesh size had been adjusted. This relative displacement is measured experimentally by two comparator pencils (Red Crown developed by Testar Marposs) (Fig. 4a). The adjustments of the relative displacements between the raceways are used mainly to verify that the mesh size of the FE model, their different coefficients of friction, and their elastic properties (E and ν) are defined perfectly. The experimental application of P on the TRB was conducted with a screw that, in turn, pushed a steel sleeve on the inner raceway, while the F_r was applied using a load cell (HBM U3 with 5 KN of capacity) (Fig. 4a). P loads were calibrated previously using a strain gauge with the same value of the preload that was acting on the TRB when it was mounted on a steel sleeve. Figure 4b shows the points where the relative displacement between the inner and outer raceway in the FE model was measured. Figure 4c also shows the differences between the relative displacements obtained from the FE models and from the test bench for the variation of P and F_r. The solid line and the dashed line show, respectively, the relative displacement obtained from the FE models and that obtained experimentally. From these pairs of curves, it can be seen that the difference between the relative displacements obtained (one from the FE models and one from the test bench) are similar. Also, Fig. 4b shows that the greater relative displacement occurred when the lower P was applied, and the minimum relative displacement was obtained when the higher P was applied. Moreover, it is seen in this figure that the greater the preload applied is, the greater is the stiffness of the mechanical contacts and the lower is the deformation of the mechanical device. This stiffness variation is in good

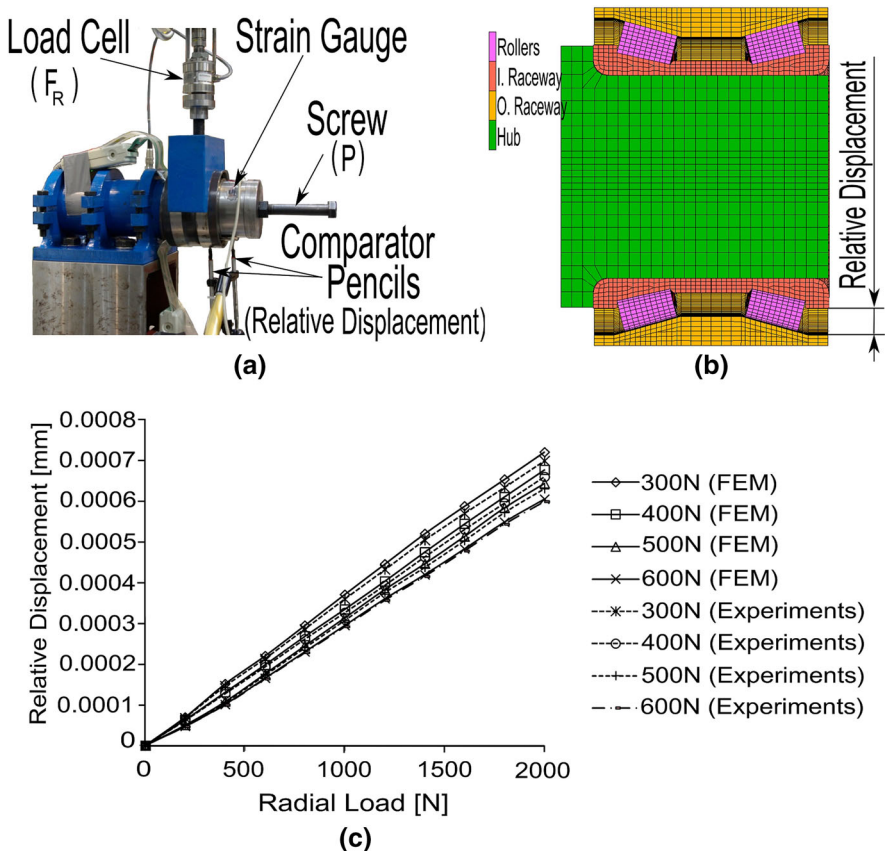

Fig. 4 **a** Test bench for the TRB: assembly of the comparators pencils, strain gauge and load cell. **b** FE model to measure the relative displacement between raceways. **c** Relative displacement of the FE model and experimental data for different values of *P*

agreement with the load–deflection relationship that was previously reported in the literature by Kania (2006) and Harris and Kotzalas (2006).

The relative displacements obtained from the FE models were consistent with the experiments and the preset parameters in the FE model ($E_{bearing} = 200$ GPa, $E_{hub} = 208$ GPa, $\nu = 0.29$, coefficient of friction $= 0.001$ and 0.2) when the mesh size is considered to be valid as explained previously.

2.3 Operating conditions for double-row TRB

Double-row TRBs are mechanical devices that are designed to support the combination of the P, F_a, F_r and T loads (Fig. 5). Due to this combination of loads, the TRB is subjected to contact normal stresses and local deformations on the different parts of the mechanical device (tapered rollers and outer and inner raceway). Also, the inner raceway is able to move a gap δ along the axis where the bearing is mounted. This gap is the distance that allows the TRB to maintain a preset value of P.

Depending on how the loads that are acting on the TRB are combined, the distribution of contact normal stresses, localized normal deformations, and the gap δ can produce values that are undesirable for the functioning of the mechanical device (Harris and Kotzalas 2006). Thus, for example, if the value of the external loads applied to the TRB corresponds to the standard values provided by the manufacturer, the distribution of normal contact stresses on the outer raceway will usually be similar to that shown in Fig. 6a. In this case, since both the top and bottom zones of the outer raceway show a non-zero value for normal contact stresses, all rollers maintain mechanical contact with the raceways at all times. If the mechanical contact of the rotating parts (tapered rollers and outer and inner raceway) is always maintained, the operating conditions of the TRB are correct and follow the manufacturer specifications.

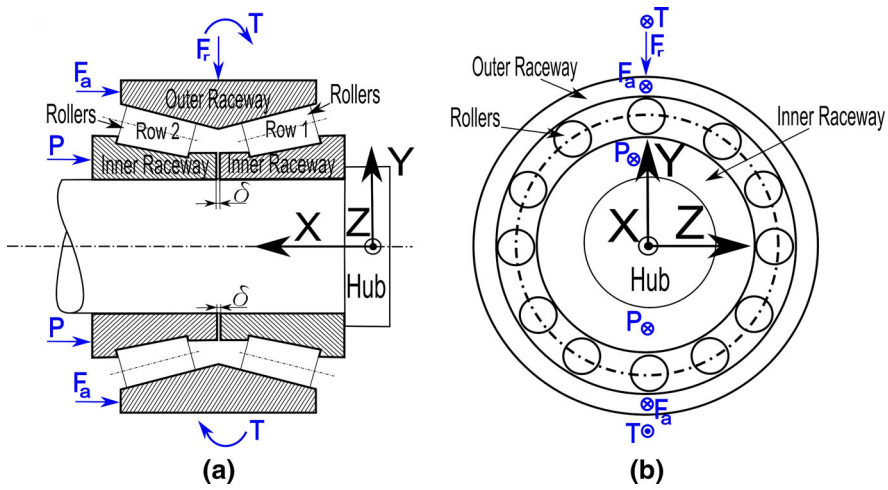

Fig. 5 Main components of a typical TRB and the corresponding loads acting on it: **a** Lateral view **b** Frontal view

In contrast, if the values of the external loads that was applied to the TRB were incorrect (i.e., a highly reduced P combined with a very high F_r and T), the distributions of contact normal stresses on the outer raceway usually would be similar to that shown in Fig. 6b. According to Fig. 6b, the top zone of the outer raceway had a non-zero value for normal contact stresses, whereas the bottom zone of the outer raceway had a zero value for normal contact stresses. In this condition, only a reduced number of rollers in the top zone maintained mechanical contact with the raceways, which can cause the rollers to detach from the outer raceway (Harris and Kotzalas 2006). Also, when the values of the external loads that are applied to the TRB correspond to the standard values that the manufacturer provided, the gap δ on the top (δ_{top}) and the bottom (δ_{bottom}) should have been the same (Fig. 6c). In contrast, if the values of the applied external loads on the TRB were incorrect (i.e., a highly reduced P combined with a very high T), the gap on the top (δ_{top}) and the bottom (δ_{bottom}) would have been different, which would have caused faulty operation of the TRB (Fig. 6d). In addition, an excessive local deformation on the outer raceway can cause undesirable effects, such as pitting and fatigue spalling of the TRB (Harris and Kotzalas 2006; Eschmann et al. 1985). According to these three requirements, we considered in this paper the following conditions for optimal operation of the TRB:

(i) The contact ratio obtained between the normal top contact stress (S_{top}) and normal bottom contact stress(S_{bottom}) on the outer raceway and for each of the two columns of rollers should be higher than 20 % to prevent detachment of the rollers in the TRB [Eq. (12)] (Harris and Kotzalas 2006).

$$\text{Contact ratio } (S) = \frac{S_{top}}{S_{bottom}} \cdot 100 \tag{12}$$

(ii) The difference between the gaps δ_{top} and δ_{bottom} should be reduced as much as possible to prevent a forced TRB operation [Eq. (13)] or misalignment (Harris and Kotzalas 2006).

$$\text{Gap difference } (\Delta\delta) = \delta_{top} - \delta_{bottom} \tag{13}$$

(iii) The localized normal deformation of the outer raceway must not exceed the maximum elastic deformation (α_{max}) of the contact zone with regard to the diameter of the tapered rolling (d) according to Eq. (14) to avoid pitting and fatigue spalling (Eschmann et al. 1985).

$$\alpha_{max} = 0.0001 \cdot d \tag{14}$$

In this case, the minimum diameter of the tapered roller is 11.3 mm. Therefore, the value of α_{max} must not exceed any point on the outer raceway by more than 0.0013.

In this work, the optimal operating condition in a double-row TRB is considered to have been reached when:

- The contact stress radio obtained for both rows of rollers (S_1 and S_2) should be between 25 and 50 %.
- The difference between the gaps obtained in the top and bottom sides of the inner raceways (δ_{top}

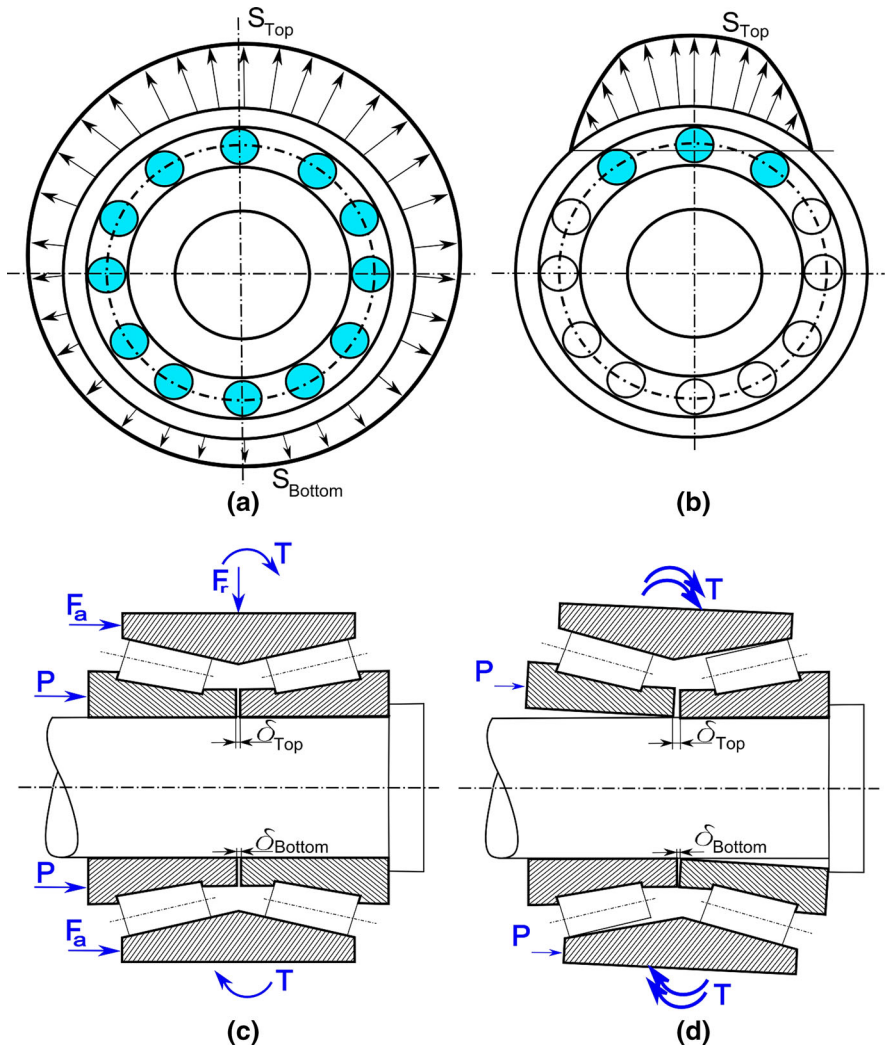

Fig. 6 Distribution of contact stresses on the outer raceway when: **a** the takeoff of the rollers does not occur **b** the takeoff of the rollers does occurs. δ_{top} and δ_{bottom} when the external loads applied to the TRB are for: **c** standard values and **d** incorrect values (Harris and Kotzalas 2006)

and δ_{bottom}) or misalignment have been reduced as much as possible.

- The local deformation on the contact surface of outer raceway (α_{max}) does not exceed the maximum elastic deformation value of 0.00113.

2.4 Design of experiments and design matrix

All statistical methods need a previously decided set of Design of Experiments (DoE) to determine the minimum number of experiments needed to fully consider the space of possibilities and ensure that the data obtained from the experiments is representative to support the hypotheses proposed (Fisher 1935). In general, the initial hypotheses are defined when a number of controllable variables (inputs or design factors) and uncontrollable variables (noise factors) determine the number of responses (outputs) by a continuous and differentiable function (Box and Behnken 1960; Taguchi 1986). There are many methods available to develop a DoE, but all this methods involve the construction of a design matrix, in which inputs and outputs are considered. One of the most widely used methods to develop a DoE is the full factorial design method (Montgomery 2008). Using this method, the experiments can adopt all possible combinations for each of the values (or levels) and each of the factors. Specially, a 2^k factorial design is a particular, full factorial design that has two levels and generates 2^k experiments, where k is the number of

Table 2 Independent variables and experimental design levels used with the CCD method

Factors	Notation	Magnitude	Levels		
			−1	0	+1
Preload	P	N	8,000	9,000	10,000
Radial load	F_r	N	60,000	80,000	100,000
Axial load	F_a	N	−200	200	600
Torque	T	N mm	−100,000	0	100,000

factors. Using this method in the optimization of the proposed TRB, the number of factors is k = 4 (P, F_r, F_a, and T) and the number of experiments or FE simulations needed is 16. This limited number of experiments or FE simulations is not enough to cover the entire space of possibilities and, subsequently, to obtain accurate regression models with which to search for the optimal operating condition for a double-row TRB. However, a factorial design 3K generates 3^k experiments or 81 FE simulations. This amount of data may be sufficient to cover completely the entire space of possibilities, but has the disadvantage of generating a large number of experiments or FE simulations. In this work, the DoE was performed using Central Composite Design (CCD). This method is considered to be a fractional three-level design that is useful in obtaining quadratic regression models, thereby reducing the number of experiments in comparison to a factorial design 3^k. Table 2 shows the values of the variables, their code, and the levels needed to implement the DoE based on CCD method.

Once the factors and levels have been set as in Table 2, the design matrix and their corresponding combination of operating conditions are generated using the "R" statistical software and subsequently simulated in the FE models (R 2014). In this case, 25 experiments or FE simulations are needed to cover the entire space of possibilities and to subsequently search for the optimal operating condition for a double-row TRB. The design matrix (See Table 3) shows the number of experiments or FE simulations and the corresponding values for the operating conditions (P, F_r, F_a, and T).

3 Results

3.1 Results obtained from the FE models

Once the FE models had been validated, an automatic procedure was performed on parameterized FE models in order to run the 25 simulations according to the design matrix. The results of these FE simulations are shown in Table 4 [contact ratio for the first row of

Table 3 Design matrix with the combination of operating conditions (inputs) to be simulated

Run	P [N]	F_r [N]	F_a [N]	T [N mm]	Run	P [N]	F_r [N]	F_a [N]	T [N mm]
1	8,000	60,000	−200	−100,000	14	9,000	80,000	200	100,000
2	8,000	60,000	−200	100,000	15	9,000	80,000	600	0
3	8,000	60,000	600	−100,000	16	9,000	100,000	200	0
4	8,000	60,000	600	100,000	17	10,000	60,000	−200	−100,000
5	8,000	80,000	200	0	18	10,000	60,000	−200	100,000
6	8,000	100,000	−200	−100,000	19	10,000	60,000	600	−100,000
7	8,000	100,000	−200	100,000	20	10,000	60,000	600	100,000
8	8,000	100,000	600	−100,000	21	10,000	80,000	200	0
9	8,000	100,000	600	100,000	22	10,000	100,000	−200	−100,000
10	9,000	60,000	200	0	23	10,000	100,000	−200	100,000
11	9,000	80,000	−200	0	24	10,000	100,000	600	−100,000
12	9,000	80,000	200	−100,000	25	10,000	100,000	600	100,000
13	9,000	80,000	200	0	–	–	–	–	–

Table 4 Results obtained from the FE models using the inputs of Table 3

Run	S_1 [%]	S_2 [%]	α_{max}	$\Delta\delta$ [mm]	Run	S_1 [%]	S_2 [%]	α_{max}	$\Delta\delta$ [mm]
1	24.74	24.66	−0.00091	0.0345	14	33.37	29.97	−0.00064	0.0216
2	19.23	30.69	−0.00131	0.0329	15	24.69	39.37	−0.00064	0.0197
3	26.65	23.16	−0.00094	0.0361	16	35.98	27.77	−0.00063	0.0233
4	20.86	29.84	−0.00097	0.0344	17	27.06	37.59	−0.00067	0.0209
5	40.09	39.72	−0.00067	0.0217	18	21.52	24.59	−0.00075	0.0276
6	32.08	49.86	−0.00070	0.0197	19	19.92	23.02	−0.00126	0.0327
7	42.40	38.06	−0.00070	0.0228	20	30.70	32.05	−0.00064	0.0204
8	34.34	48.15	−0.00073	0.0212	21	27.70	34.71	−0.00080	0.0254
9	28.53	33.81	−0.00081	0.0266	22	29.63	26.87	−0.00077	0.0291
10	20.54	17.68	−0.00089	0.0355	23	25.56	30.45	−0.00078	0.0266
11	15.77	23.15	−0.00089	0.0339	24	22.73	35.12	−0.00080	0.0272
12	21.60	17.36	−0.00125	0.0366	25	26.40	29.66	−0.00079	0.0268
13	16.43	21.85	−0.00128	0.0343	–	–	–	–	–

rollers (S_1), contact ratio for the second row of rollers (S_2), maximum normal deformation (α_{max}), and gap difference ($\Delta\delta$)].

3.2 Analysis of variance

Equation (2) was fitted using the data shown in Tables 3 and 4 to obtain the regression equations for all responses with the use of the RMS "R" package (Lenth 2009). Second order polynomial models were built for each response, and several criteria (R^2, p value, MAPE and RMSE) were used to select the most accurate model.

Equations (17), (18), (19) and (20) show the second degree polynomial function obtained to model S_1, S_2, α_{max} and $\Delta\delta$.

$$\begin{aligned} S_1 = & -0.3553 + 0.00013 \cdot P - 4.2 \cdot 10^{-9} \cdot P^2 \\ & + 4.14 \cdot 10^{-7} \cdot F_r - 3 \cdot 10^{-10} \cdot P \cdot F_r \\ & - 1.4174 \cdot 10^{-5} \cdot F_r + 2.2 \cdot 10^{-9} \cdot P \cdot F_a \\ & - 3 \cdot 10^{-10} \cdot F_r \cdot F_a + 1.001 \cdot 10^{-7} \cdot F_a^2 \\ & - 6.593 \cdot 10^{-7} \cdot T \end{aligned} \quad (15)$$

$$\begin{aligned} S_2 = & -0.7544 + 0.00015 \cdot P - 4.2 \cdot 10^{-9} P^2 \\ & + 8.2536 \cdot 10^{-6} F_r - 4 \cdot 10^{-10} P F_r \\ & - 1 \cdot 10^{-10} F_r^2 - 0.000106 \cdot F_a \\ & - 2 \cdot 10^{-10} \cdot P \cdot F_a + 3 \cdot 10^{-10} \cdot F_r \cdot F_a \\ & + 1.604 \cdot 10^{-7} \cdot F_a^2 + 5.987 \cdot 10^{-7} \cdot T \end{aligned} \quad (16)$$

$$\begin{aligned} \alpha_{max} = & 0.001693 - 7.29 \cdot 10^{-7} \cdot P + 3.37 \cdot 10^{-8} \cdot F_r \\ & - 1.3504 \cdot 10^{-6} \cdot F_a + 2 \cdot 10^{-10} \cdot P \cdot F_a \\ & + 1 \cdot 10^{-10} \cdot F_a^2 + 2.9 \cdot 10^{-9} \cdot T \end{aligned} \quad (17)$$

$$\begin{aligned} \Delta\delta = & 0.03729 - 9.0738 \cdot 10^{-6} \cdot P + 5 \cdot 10^{-10} \cdot P^2 \\ & + 4.363 \cdot 10^{-7} \cdot F_r + 1.5571 \cdot 10^{-6} \cdot F_a \\ & + 2 \cdot 10^{-10} \cdot P \cdot F_a - 3.1 \cdot 10^{-9} \cdot F_a^2 \\ & - 1.81 \cdot 10^{-8} \cdot T \end{aligned} \quad (18)$$

These equations show how each output was defined by first and second degree polynomials. Then, ANOVA was used to reduce the size of these regression models by removing the insignificant terms of the polynomial (Sathiya et al. 2006). This method, called step-wise regression, automatically removes the features of no significance for each model (Wilkinson and Dallal 1981). Equations (19), (20), (21) and (22) show the reduced quadratic models.

$$\begin{aligned} S_1 = & -0.004182 + 5.66892 \cdot 10^{-5} \cdot P \\ & - 3 \cdot 10^{-10} \cdot P \cdot F_r - 3 \cdot 10^{-10} \cdot F_r \cdot F_a \\ & + 1.078 \cdot 10^{-7} \cdot F_a^2 - 6.54 \cdot 10^{-7} \cdot T \end{aligned} \quad (19)$$

$$\begin{aligned} S_2 = & -0.434307 + 7.55976 \cdot 10^{-5} \cdot P \\ & + 8.7701 \cdot 10^{-6} \cdot F_r - 4 \cdot 10^{-10} \cdot P \cdot F_r \\ & - 1 \cdot 10^{-10} \cdot F_r^2 - 8.39731 \cdot 10^{-5} \cdot F_a \\ & + 1.532 \cdot 10^{-7} \cdot F_a^2 + 8.1 \cdot 10^{-7} \cdot T \end{aligned} \quad (20)$$

$$\alpha_{max} = 0.000546 - 1.685 \cdot 10^{-7} \cdot P - 1.5291 \cdot 10^{-6} \cdot F_a + 2 \cdot 10^{-10} \cdot P \cdot F_a \quad (21)$$

$$\Delta\delta = 0.036197 - 8.4334 \cdot 10^{-6} \cdot P + 5 \cdot 10^{-10} \cdot P^2 + 3.95 \cdot 10^{-7} \cdot F_r + 3 \cdot 10^{-10} \cdot P \cdot F_a - 3.1 \cdot 10^{-9} \cdot F_a^2 - 9.5 \cdot 10^{-9} \cdot T \quad (22)$$

Tables 5, 6, 7 and 8 show the results of ANOVA for each of the final quadratic models. Most of the variables have a p value that is less than 0.01. This indicates that the variables used on the reduced quadratic models are statistically significant. The multiple correlation coefficient (R^2) is calculated as the measure of the amount of variation around the mean obtained by the regression model. The results showed that all values of R^2 are close to 1, which indicates that these models possess a good predictive capacity.

MAPE and RMSE are calculated to determine the generalization capacity of the reduced quadratic

Table 5 ANOVA results for the variable S_1 using the final reduced quadratic model

Var.	Df	Sum of Sq.	Mean square	F value	p value	Sig. code
P	1	0.014995	0.014995	268.215	2.940 E−12	***
P·F_r	1	0.074119	0.074119	1325.801	<2.20 E−16	***
F_r·F_a	1	0.000815	0.000815	14.575	0.0012606	**
$(F_a)^2$	1	0.001781	0.001781	31.861	2.350 E−05	***
T	1	0.021224	0.021224	379.645	1.510 E−13	***
F_r·T	1	0.000965	0.000965	17.257	0.0005959	***
Residuals	18	0.001006	0.000056			
R^2	0.992					

Significance codes: 0 '***' 0.001 '**' 0.01 '*' 0.05 '.' 0.1 '' 1

Table 6 ANOVA results for the variable S_2 using the final reduced quadratic model

Var.	Df	Sum of sq.	Mean square	F value	p value	Sig. code
P	1	0.034339	0.034339	192.6450	5.78 E−10	***
F_r	1	0.095544	0.095544	536.0037	3.74 E−13	***
P·F_r	1	0.001019	0.001019	5.7159	0.030366	*
$(F_r)^2$	1	4.45 E−7	4.45 E−7	0.0025	0.960409	
F_a	1	0.001485	0.001485	8.3334	0.011294	*
$(F_a)^2$	1	0.002739	0.002739	15.3680	0.001364	**
T	1	0.027512	0.027512	154.3425	2.69 E−09	***
F_r·T	1	0.001756	0.001756	9.8534	0.006757	**
$(T)^2$	1	0.000434	0.000434	2.4349	0.139507	
Residuals	15	0.002674	0.000178			
R^2	0.983					

Significance codes: 0 '***' 0.001 '**' 0.01 '*' 0.05 '.' 0.1 '' 1

Table 7 ANOVA results for the variable α_{max} using the final reduced quadratic model

Var.	Df	Sum of sq.	Mean square	F value	p value	Sig. code
P	1	3.80 E−10	3.80 E−10	0.0357	8.52 E−01	
P·F_r	1	7.22 E−07	7.22 E−07	68.1084	1.56 E−07	***
$(F_r)^2$	1	6.87 E−08	6.87 E−08	6.4767	0.02031	*
F_a	1	1.47 E−08	1.47 E−08	1.3816	0.25515	
P·F_a	1	6.72 E−08	6.72 E−08	6.3315	0.02157	*
P·T	1	2.14 E−08	2.14 E−08	2.0147	0.17287	
Residuals	18	1.91 E−07	1.06 E−08			
R^2	0.815					

Significance codes: 0 '***' 0.001 '**' 0.01 '*' 0.05 '.' 0.1 '' 1

Table 8 ANOVA results for the variable Δδ using the final reduced quadratic model

Var.	Df	Sum of sq.	Mean square	F value	*p* value	Sig. code
P	1	6.90 E−07	6.90 E−07	7.6861	1.36 E−02	*
$(P)^2$	1	5.78 E−06	5.78 E−06	64.7389	5.14 E−07	***
F_a	1	0.00079	0.00079	8879.0365	<2.2 E−16	***
$P{\cdot}F_r$	1	3.10 E−07	3.10 E−07	3.5204	0.07898	·
$P{\cdot}F_a$	1	7.38 E−06	7.38 E−06	82.588	1.02 E−07	***
$(F_a)^2$	1	0.18 E−08	0.18 E−08	0.0263	0.87319	
T	1	1.62 E−05	1.62 E−05	181.6036	3.77 E−10	***
$(T)^2$	1	5.96 E−06	5.96 E−06	66.6928	4.24 E−07	***
Residuals	16	1.43 E−06	9.00 E−07			
R^2	0.998					

Significance codes: 0 '***' 0.001 '**' 0.01 '*' 0.05 '.' 0.1 '' 1

Table 9 Results of the predicted error criteria for S_1, S_2, α_{max} and Δδ using the reduced quadratic models

	S_1	S_2	α_{max}	Δδ
MAPE [%]	1.87	2.78	8.06	0.71
RMSE [%]	2.28	3.22	13.29	1.46

models using the samples shown in Table 4 according to Eqs. (23) and (24).

$$MAPE = \frac{1}{m} \cdot \sum_{k=1}^{m} \left| \frac{Y_{k\,FEM} - Y_{k\text{Model}}}{Y_{k\,FEM}} \right| \tag{23}$$

$$RMSE = \sqrt{\frac{1}{m} \cdot \sum_{k=1}^{m} \left(Y_{k\,FEM} - Y_{k\text{Model}}\right)^2} \tag{24}$$

In this case, Y_{kFEM} are the normalized responses obtained from the FE models and Y_{kModel} are those obtained from the reduced quadratic models developed with RSM. The normalization of the data is commonly used in statistical processes in order to transform all variables to the same scale (from 0 to 1). In this case, this transformation is carried out subtracting the minimum value from each original value and dividing by the range of each variable according to Eq. (25).

$$Y_{k,norm} = \frac{Y_k - \min(Y)}{range(Y)} \tag{25}$$

Table 9 shows the prediction errors, where the maximum error corresponds to α_{max} (MAPE equal to 8.06 % and RMSE equal to 13.29 %), and the minimum error corresponds to $\Delta\delta$ (MAPE equal to 0.71 % and RMSE equal to 1.46 %).

Additionally, 22 new FE models were implemented to test the quadratic regression models with new operating conditions that had not been used previously to generate reduced quadratic models. The errors obtained during the testing stage are shown in Table 10, where the maximum error corresponds to S_2 (MAPE equal to 5.47 % and RMSE equal to 7.70 %), and the minimum error corresponds to Δδ (MAPE equal to 1.72 % and RMSE equal to 2.87 %).

Figure 7 shows the relationship between the actual (FEM) and predicted (reduced quadratic models) values of S_1 (Fig. 7a), S_2 (Fig. 7b), α_{max} (Fig. 7c), and Δδ (Fig. 7d). The figures show that these models are adequate to predict these values because the residuals that were obtained are small and the correlations between actual and predicted values are high.

3.3 Multi-response optimization

Table 11 shows the combination of operating conditions and outputs that were studied in searching for the optimal operating condition in a double-row TRB through desirability functions using the RMS "R" package (Kuhn 2014). The first column of this table shows the inputs and outputs that were studied. The second column of the table shows the goal set in the optimization process for both inputs and outputs. In this case, the process of searching for the best combination was accomplished by prefixing a range for the preload (between 8000 and 10,000 N), while F_r, F_a and T were analyzed for a fixed number of settings. In this case, the combination of the operating conditions F_r, F_a and T were considered to be the load capacity, while P is preset when the TRB is mounted

Table 10 Test dataset with 22 new instances

N°	P [N]	F_r [N]	F_a [N]	T [N mm]	FEM				Predicted values			
					S_1	S_2	α_{max}	$\Delta\delta$ [mm]	S_1	S_2	α_{max}	$\Delta\delta$ [mm]
1	10,000	100,000	600	0	23.43	26.15	−0.00094	0.0339	23.5	25.3	−0.0010050	0.03366
2	10,000	60,000	200	−100,000	41.41	38.93	−0.00068	0.0222	39.7	36.2	−0.0006591	0.02281
3	10,000	60,000	200	0	36.94	43.36	−0.00069	0.0198	35.5	39.9	−0.0006972	0.02040
4	10,000	60,000	200	100,000	33.39	49.02	−0.00071	0.0207	31.3	46.1	−0.0007359	0.02091
5	10,000	60,000	600	0	37.78	42.48	−0.00070	0.0199	38.2	41.5	−0.0006615	0.02066
6	10,000	80,000	−200	0	27.99	34.85	−0.00080	0.0261	29.4	37.4	−0.0008433	0.02564
7	10,000	80,000	200	−100,000	32.05	30.58	−0.00080	0.0287	31.8	31.4	−0.0007689	0.02931
8	8,470	65,350	220	37,890	27.74	34.42	−0.00069	0.0225	26.9	33.1	−0.0006862	0.02180
9	8,475	100,000	−150	−90,000	20.80	18.50	−0.00090	0.0349	21.2	19.4	−0.0010008	0.03472
10	8,530	100,000	−150	−90,000	20.88	18.62	−0.00090	0.0346	21.4	19.6	−0.0010022	0.03467
11	8,000	100,000	600	0	18.66	18.23	−0.00124	0.0338	19.2	18.2	−0.0011913	0.03408
12	8,000	60,000	200	100,000	25.72	38.75	−0.00065	0.0202	24.1	35.8	−0.0006533	0.02102
13	8,000	60,000	600	0	31.03	31.85	−0.00064	0.0207	31.0	31.1	−0.0007162	0.02052
14	8,000	80,000	200	−100,000	25.62	21.10	−0.00076	0.0289	26.0	22.7	−0.0007674	0.02970
15	8,000	80,000	200	100,000	18.47	28.81	−0.00077	0.0270	19.2	30.5	−0.0008283	0.02780
16	9,835	90,480	245	−93,315	28.20	26.39	−0.00086	0.0327	27.2	26.4	−0.0008785	0.03243
17	9,000	60,000	−200	−100,000	37.24	36.35	−0.00,064	0.0214	36.8	34.4	−0.0005975	0.02125
18	9,000	60,000	−200	0	32.78	41.15	−0.00065	0.0194	32.6	38.1	−0.0006318	0.01884
19	9,000	60,000	−200	100,000	28.82	46.63	−0.00067	0.0197	28.4	44.3	−0.0006661	0.01936
20	9,000	60,000	200	−100,000	38.24	35.44	−0.00065	0.0223	36.1	31.1	−0.0006260	0.02238
21	9,000	60,000	200	10,0000	29.74	45.83	−0.00068	0.0204	27.7	41.0	−0.0006946	0.02048
22	9,000	60,000	600	−10,0000	39.23	34.58	−0.00067	0.0228	38.8	32.6	−0.0006546	0.02252
						MAPE [%]			2.91	5.47	4.37	1.72
						RMSE [%]			3.64	7.70	9.57	2.87

Operating conditions (Inputs), FEM outputs, and predicted values used the reduced quadratic models for S_1, S_2, α_{max} and $\Delta\delta$

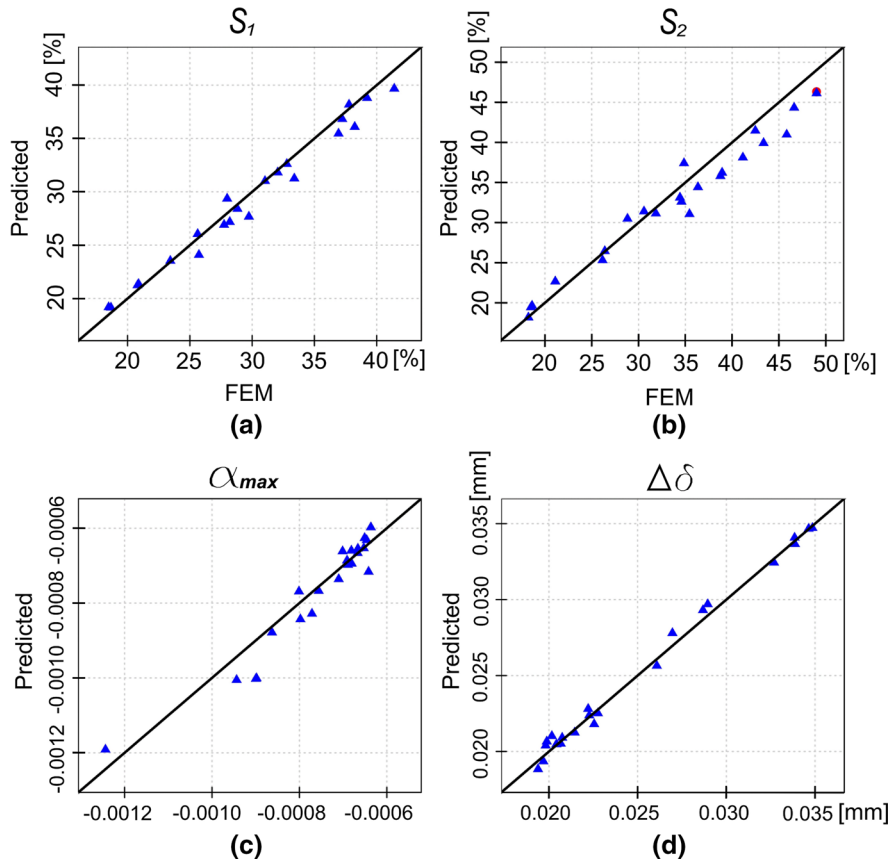

Fig. 7 Scatter diagram of: **a** contact ratio for the first row of rollers (S_1), **b** contact ratio for the second row of rollers (S_2), **c** the normal maximum deformation (α_{max}) and **d** the gap difference ($\Delta\delta$)

Table 11 Results of the optimal operating condition to obtain the requirements of S_1, S_2, α_{max} and $\Delta\delta$ (Total number of combinations studied equal to 5,31,441)

Inputs/outputs	Goal	Min.	Max.
Preload (P)	In range	8,000 N	10,000 N
Radial load (F_r)	Equal	60,000 N	100,000 N
Axial load (F_a)	Equal	−200 N	600 N
Torque (T)	Equal	−100,000 N mm	100,000 N mm
S_1	In range	20 %	50 %
S_2	In range	20 %	50 %
α_{max}	Max.	−0.0011	−0.0006
$\Delta\delta$	Min.	0.0197 mm	0.0366 mm

on the hub. Thus, for example, F_r varies from 60,000 to 100,000 N (every 500 N), F_a varies from −200 to 600 N (every 10 N) and T varies from −100,000 to 100,000 N mm (every 2500 N mm). The requirements of searching for the optimal operating condition are set between 20 and 50 % for S_1 and S_2 (goal in range), between −0.0011 and −0.0006 mm for α_{max} (goal equal to maximum), and between 0.0197 and 0.0366 mm for $\Delta\delta$ (goal equal to minimum). The combination of inputs (F_r, F_a and T) for the optimal operating condition required (S_1, S_2, α_{max} and $\Delta\delta$) involves a total of 5,31,441 different combinations with their corresponding different desirabilities.

Some of the combinations obtained to reach the optimal operating conditions according to the requirements of the TRB are shown in Table 12. Thus, for example, the first row of the table (Combination N° 1) shows the highest values of desirability (=1) when the

Table 12 Results of the operating condition necessary to reach the requirements of S_1, S_2, α_{max} and $\Delta\delta$

N°	P [N]	F_r [N]	F_a [N]	T [N mm]	S_1	S_2	α_{max}	$\Delta\delta$ [mm]	Des.
1	8666.75	6.25E + 4	−200	52,500	28.52	38.92	−0.000628534	0.019687085	1
2	8451.01	100,000	−200	−32,500	20.00	20.79	−0.001013224	0.032969024	0.199
3	9905.42	60,000	600	−15,000	38.47	40.26	−0.000661533	0.020711334	0.936
4	8605.55	60,500	−200	10,0000	26.86	42.21	−0.000628141	0.019696796	1
5	8290.67	60,000	10	97,500	25.15	38.11	−0.000630001	0.020366156	0.980
6	8211.74	60,000	210	−7,500	29.40	30.30	−0.000629997	0.020371162	0.979
7	8058.65	60,000	−200	−22,500	30.19	32.20	−0.000529044	0.019684583	1
8	8780.61	60,000	−200	45,000	29.93	39.47	−0.000625727	0.018761519	1
9	8945.34	10,0000	500	10,0000	17.68	24.81	−0.001132020	0.034019252	0

load capacity of the TRB is the maximum (F_r, F_a and T), while P can reach any value (P = 8666.75 N; F_r = 62,500 N; F_a = −200 N, and T = 52,500 N mm). Also, if the value of F_r is the maximum when the values of F_a and T are the maximum negatives values (Combination N° 2), P = 8451.01 N and the desirability is equal to 0.199. This combination of operating conditions shows that for large values of F_r, the desirability values obtained are lower. In contrast, if the values of F_a are the maximum and minimum possible for any of the values of F_r and T, the values obtained for P and for the desirability are, respectively, 9905.42 and 0.936 (N° 3) and 8605.55 and 1 (N° 4). Furthermore, the combinations N° 5, 6, 7 and 8 show the operating condition when the values of S_1, S_2, α_{max} and $\Delta\delta$ are the lowest. Also, these four combinations of operating conditions show high values of desirability. Finally, the combination N° 9 has a desirability value equal to zero when the values of F_r, F_a and T are the highest.

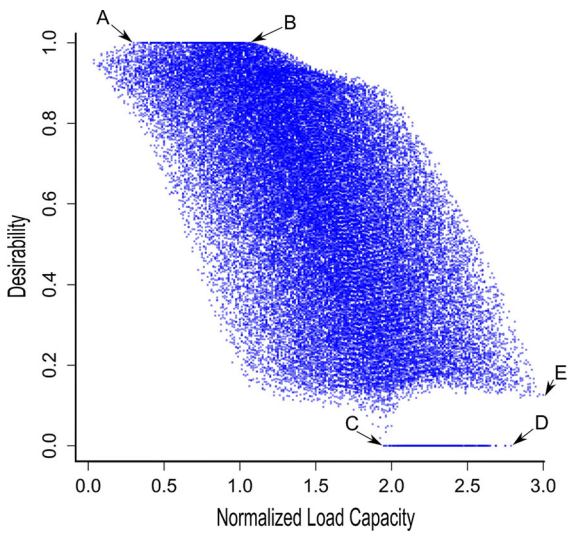

Fig. 8 Desirability function versus the normalized load capacity

Figure 8 shows the desirability function versus the normalized load capacity used to obtain the requirements with the optimal operating conditions based on combinations from Table 11. In this case, the normalized load capacity is defined as the sum of the normalized values that correspond to F_a, F_r and T [Eq. (26)].

$$LC_{norm} = F_{anorm} + F_{rnorm} + T_{norm} \tag{26}$$

Each one of the normalized values of F_a, F_r and T are calculated using Eq. (25). Figure 8 shows that the optimal operating condition to obtain the requirements of S_1, S_2, α_{max} and $\Delta\delta$ (desirability equal to 1) is reached for a reduced number of combinations (top line from point A to point B). In this case, point A corresponds to the minimum values of normalized load capacity (P = 8694.88 N; F_r = 60,000 N; F_a = 0 N and T = 0 N mm), and point B corresponds to the maximum values of normalized load capacity (P = 8666.75 N; F_r = 62,500 N; F_a = −200 N and T = 52,500 N mm). In contrast, the lower line (from point C to point D) corresponds to the worst operating condition to obtain the requirements (equal desirability to 0). Point C corresponds to values of the minimum load capacity (P = 8087.38 N; F_r = 96,000 N; F_a = −200 N and T = 52,500 N mm), and point D corresponds to values of the maximum load capacity (P = 8058.11 N; F_r = 100,000 N; F_a = −200 N and T = 100,000 N mm).

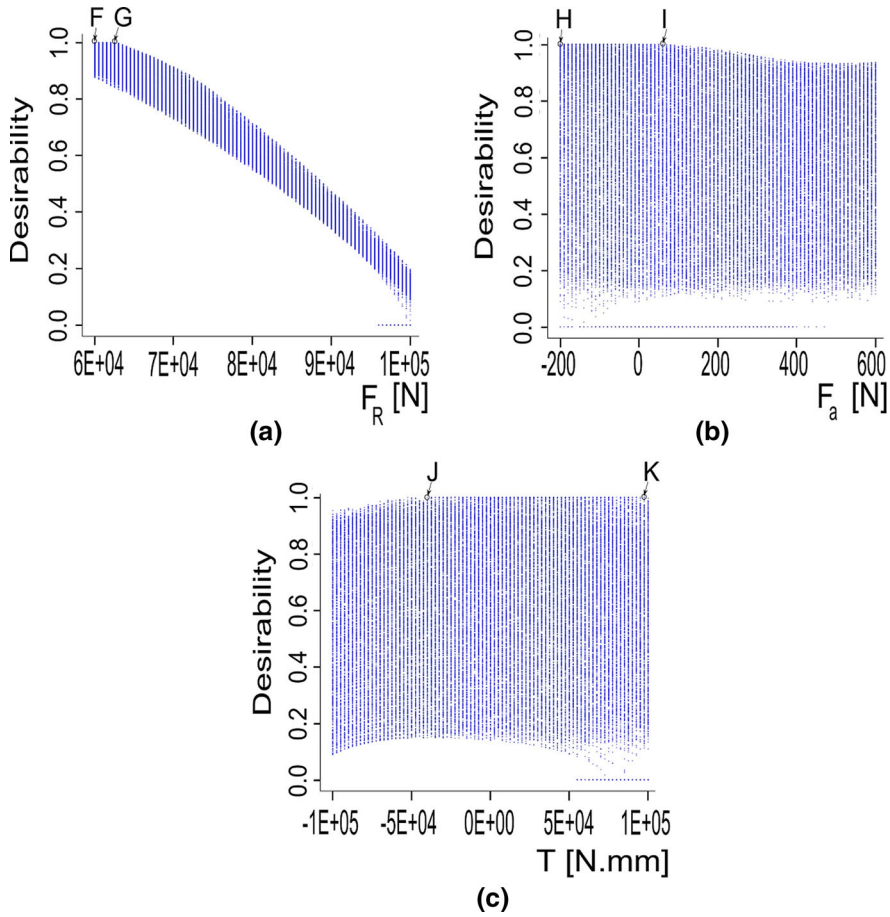

Fig. 9 Desirability function versus **a** F_r, **b** F_a, and **c** T

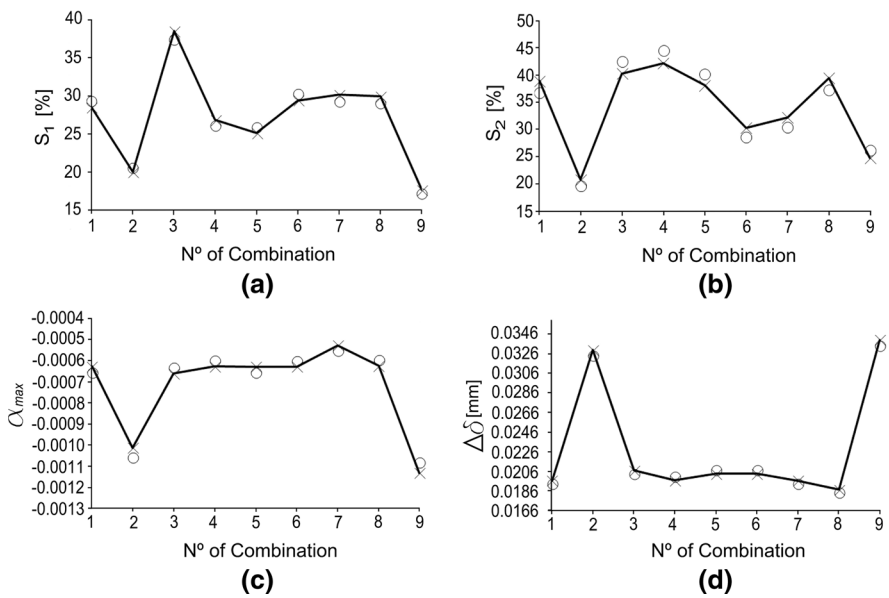

Fig. 10 Comparison of the predictions of S_1, S_2, α_{max} and $\Delta\delta$ using the RSM method (*cross*) and FE method (*open circle*)

Finally, point E corresponds to the combination of the maximum load capacity (P = 9999.87 N; F_r = 100,000 N; F_a = 600 N and T = 100,000 N mm), which corresponds to a desirability value of 0.126.

Figure 9 shows the desirability function versus several loads: F_r (Fig. 9a), F_a (Fig. 9b) and T (Fig. 9c). The desirability function may achieve maximum values equal to 1 in a reduced range of F_r (from point F (60,000 N) to point G (62,500 N) in Fig. 9a), in a wider range of F_a (from point H (−200 N) to point I (70 N) in Fig. 9b), and in a wider range of T (from point J (50,000 N) to point K (100,000 N) in Fig. 9c). Finally, from these figures one can see that the maximum values of the desirability function are achieved only for values of F_r that are close to the minimum of its range.

Finally, in this work, several more FE simulations are conducted with some of the optimized operating conditions in order to compare the FE results to the predicted ones. Figure 10 provides, for some of the optimal operating conditions shown in Table 12, a comparison between the values of S_1, S_2, α_{max} and $\Delta\delta$ obtained from the RSM method and the values obtained from the FE model.

This figure clearly shows that the errors in the prediction of S_2 obtained with the RSM method (MAPE equal to 5.45 %) with respect to the values obtained from the FE model are higher than with the other parameters (MAPE for S_1 equal to 2.92 %, for α_{max} equal to 4.4 % and for $\Delta\delta$ equal to 1.76 %).

4 Conclusion

It has been clearly demonstrated that a combination of FEM and MRS optimization can be used to search for the optimal operating condition in the design phase of double-row TRB. The FEM has been used successfully to simulate the TRB and a good agreement between simulations and experiments has been obtained. Then, the validated FE models are used to generate three of the most important parameters of the TRB design, which was used subsequently to develop quadratic regressions models. In order to check their generalization ability, these quadratic regressions models were tested with new operating condition. Several error criteria were calculated. In addition, a multi-response optimization study was conducted using a desirability approach and based on the reduced quadratic regressions models obtained. The optimization results indicated that the optimal operating conditions, which are P = 8666.75 N; F_r = 62,500 N; F_a = −200 N and T = 52,500 N mm, correspond to the maximum load capacity for the range of operating conditions preset. The study also showed that, for the range of preset operating conditions, the combination that makes the load capacity maximum does not obtain the requirements for which the TRB has been designed. Finally, from the results obtained, it is concluded that combining FEM and MRS optimization can be used successfully in the design of any mechanical device.

Conflict of interests The authors declare that there is no conflict of interests regarding the publication of this paper.

References

Arora, V., van der Hoogt, P.J.M., Aarts, R.G.K.M., de Boer, A.: Identification of stiffness and damping characteristics of axial air-foil bearings. Int. J. Mech. Mater. Des. **7**(3), 231–243 (2011)

Arora, V., Van der Hoogt, P.J.M., Aarts, R.G.K.M., de Boer, A.: Identification of dynamic properties of radial air-foil bearings. Int. J. Mech. Mater. Des. **6**(4), 305–318 (2010)

Azaouzi, M., Lebaal, N., Rauchs, G., Belouettar, S.: Optimal design of multi-step stamping tools based on response surface method. Simul. Model. Pract. Theory **24**, 1–14 (2012)

Bahloul, R., Mkaddem, A., Dal Santo, P.: Sheet metal bending optimization using response surface method, numerical simulation and design of experiments. Int. J. Mech. Sci. **48**(9), 991–1003 (2006)

Borgelt, C., Gil, M.Á., Sousa, J.M., Verleysen, M.: Towards Advanced Data Analysis by Combining Soft Computing and Statistics. Springer, Berlin (2013)

Box, G.E., Behnken, D.W.: Some new three level designs for the study of quantitative variables. Technometrics **2**(4), 455–475 (1960)

Box, G.E., Wilson, K.B.: On the experimental attainment of optimum conditions. J. R. Stat. Soc. A. Stat. **13**(1), 1–45 (1951)

del Coz Diaz, J.J., Garcia-Nieto, P.J., Alvarez-Rabanal, F.P., Alonso-Martínez, M., Dominguez-Hernandez, J., Perez-Bella, J.M.: The use of response surface methodology to improve the thermal transmittance of lightweight concrete hollow bricks by FEM. Constr. Build. Mater. **52**, 331–344 (2014)

Demirhan, N., Kanber, B.: Stress and displacement distributions on cylindrical roller bearing rings using FEM. Mech. Based Des. Struct. **36**(1), 86–102 (2008)

Derringer, G., Suich, R.: Simultaneous optimization of several response variables. J. Qual. Technol. **12**, 214–219 (1980)

Di Lorenzo, R., Ingarao, G., Chinesta, F.: Integration of gradient based and response surface methods to develop a cascade

optimisation strategy for Y-shaped tube hydroforming process design. Adv. Eng. Softw. **41**(2), 336–348 (2010)
El-Abbasi, N., Bathe, K.J.: Stability and patch test performance of contact discretizations and a new solution algorithm. Comput. Struct. **79**(16), 1473–1486 (2001)
Eschmann, P., Hasbargen, L., Weigand, K.: Ball and roller bearings: theory, design, and application. R. Oldenbourg, Munich (1985)
Escribano, R., Lostado, R., Fernández, R., Villanueva, P., Mac Donald, B.J.: Improvement in Manufacturing Welded Products Through Multiple Response Surface Methodology and Data Mining Techniques. International Joint Conference SOCO'14-CISIS'14-ICEUTE'14, pp. 301–310. Springer International Publishing, Berlin (2014)
Feng, Q., Prinja, N.K.: NAFEMS Benchmark Tests for Finite Element Modelling of Contact. Gapping and Sliding, NAFEMS, Report (2001). **R0081**
Fisher, R.A.: The Design of Experiments. Oliver and Boyd, Oxford (1935)
Gelman, A.: Analysis of variance? Why it is more important than ever. Ann. Stat. **33**(1), 1–53 (2005)
Guo, Y., Parker, R.G.: Stiffness matrix calculation of rolling element bearings using a finite element/contact mechanics model. Mech. Mach. Theory **51**, 32–45 (2012)
Harrington, E.C.: The desirability function. Ind. Qual. Control **21**(10), 494–498 (1965)
Harris, T.A., Kotzalas, M.N.: Essential Concepts of Bearing Technology. Taylor and Francis, New York (2006)
Hertz, H.: On the Contact of Rigid Elastic Solids and on Hardness, in Miscellaneous Papers. MacMillan, London (1896)
Illera, M., Lostado, R., Fernandez, R., MacDonald, B.: Characterization of electrolytic tinplate materials via combined finite element and regression models. J. Strain Anal. Eng. **49**(6), 467–480 (2014)
Kania, L.: Modelling of rollers in calculation of slewing bearing with the use of finite elements. Mech. Mach. Theory **41**(11), 1359–1376 (2006)
Kelly, D.W., Gago, D.S., Zienkiewicz, O.C., Babuska, I.: A posteriori error analysis and adaptive processes in the finite element method: part I—Error analysis. Int. J. Numer. Methods Eng. **19**(11), 1593–1619 (1983)
Kuhn, M.: Desirability: desirabiliy function optimization and ranking. R package v.1.6. http://CRAN.R-project.org/package=desirability (2014)
Lenth, R.V.: Response-surface methods in R using RSM. J. Stat. Softw. **32**(7), 1–17 (2009)
Lostado, R., Escribano, R., Fernández, R., Illera, M., Mac Donald, B.J.: Combination of the Finite Element Method and Data Mining Techniques to Design and Optimize Bearings. International Joint Conference SOCO'14-CISIS'14-ICEUTE'14, pp. 165–174. Springer International Publishing, Berlin (2014)
Lostado, R., Martínez De Pisón, F.J., Pernía, A., Alba, F., Blanco, J.: Combining regression trees and the finite element method to define stress models of highly non-linear mechanical systems. J. Strain Anal. Eng. **44**(6), 491–502 (2009)
Lundberg, G., Sjövall, H. Stress and Deformation in Elastic Contacts, Publication no. 4. Institute of Theory of Elasticity and Strength of Materials, Chalmers Institute Technology, Gothenburg (1958)
Marwala, T.: Finite-element-model Updating Using Computational Intelligence Techniques: Applications to Structural Dynamics. Springer, Amsterdam (2010)
Meguid, S.A., Czekanski, A.: Advances in computational contact mechanics. Int. J. Mech. Mater. Des. **4**(4), 419–443 (2008)
Montgomery, D.C.: Design and Analysis of Experiments. John, New Jersey (2008)
MSC Marc User's Guide Version 2010. MSC Software Corporation LA (2010)
Myers, R.H.: Response surface methodology. Allyn-Bacon, Boston (1971)
Nagatomo, T., Takahashi, K., Okamura, Y., Kigawa, T., Noguchi, S.: Effects of load distribution on life of radial roller bearings. J. Tribol. **134**(2), 021101 (2012)
R Core Team.: R: A language and environment for statistical computing. R Foundation for statistical computing. http://www.R-project.org/ (2014)
Sathiya, P., Aravindan, S., Haq, A.N.: Optimization for friction welding parameters with multiple performance characteristics. Int. J. Mech. Mater. Des. **3**(4), 309–318 (2006)
Satyanarayana, S., Melkote, S.N.: Finite element modeling of fixture-workpiece contacts: single contact modeling and experimental verification. Int. J. Mach. Tool Manuf. **44**(9), 903–913 (2004)
Shigley, J.E., Mischke, C.R., Budynas, R.G.: Mechanical Engineering Design. Mc. Graw Hill, New York (2004)
Taguchi, G.: Introduction to Quality Engineering: Designing Quality into Products and Processes. Quality Resources, New York (1986)
Wilkinson, L., Dallal, G.E.: Tests of significance in forward selection regression with an F-to enter stopping rule. Technometrics **23**(4), 377–380 (1981)
Yanhui, Y., Dong, L., Ziyan, H., Zijian, L.: Optimization of preform shapes by RSM and FEM to improve deformation homogeneity in aerospace forgings. Chin. J. Aeronaut. **23**(2), 260–267 (2010)
Zavarise, G., De Lorenzis, L.: A modified node-to-segment algorithm passing the contact patch test. Int. J. Numer. Meth. Eng. **79**(4), 379–416 (2009)
Zeng, G., Li, S.H., Yu, Z.Q., Lai, X.M.: Optimization design of roll profiles for cold roll forming based on response surface method. Mater. Des. **30**(6), 1930–1938 (2009)
Zhang, X.P., Ahmed, H., Yao, Z.: Multi-body contact modeling and statistical experimental validation for hub-bearing unit. Tribol. Int. **36**(7), 505–510 (2003)